École doctorale nº 364 : Sciences Fondamentales et Appliquées

Doctorat ParisTech

T H È S E

pour obtenir le grade de docteur délivré par

l'École Nationale Supérieure des Mines de Paris

Spécialité doctorale "Science et Génie des Matériaux"

présentée et soutenue publiquement par

Ali SAAD

le 09 février 2016

NUMERICAL MODELLING OF MACROSEGREGATION FORMED DURING SOLIDIFICATION WITH SHRINKAGE USING A LEVEL SET APPROACH

Co-directeur de thèse: **Charles-André GANDIN**
Co-directeur de thèse: **Michel BELLET**

Jury

Pr. Hervé COMBEAU,	Professeur, Ecole des Mines de Nancy, France	
Pr. Markus RETTENMAYR,	Professeur, Université de Jena, Allemagne	
Pr. Florian KARGL,	Professeur, Agence Spatiale Allemande (DLR), Allemagne	
Dr. Charles-André GANDIN,	Directeur de recherche, CNRS, France	Examinateur
Pr. Michel BELLET,	Professeur MINES ParisTech, France	Examinateur
Dr. Frédéric COSTES,	Chef de service *THERCAST*®, TRANSVALOR S.A., France	Invité

MINES ParisTech
Centre de Mise en Forme des Matériaux (CEMEF)
UMR CNRS 7635, F-06904 Sophia Antipolis, France

T
H
E
S
E

Acknowledgement

Dedicated to humanity ...

Contents

Contents

List of Acronyms

Acronym	Standing for
ALE	Arbitrary Lagrangian-Eulerian
BTR	Brittle temperature range
CAFD	Cellular Automata Finite Difference
CAFE	Cellular Automata Finite Element
CBB	Circumventing Babuška-Brezzi
CCEMLCC	Chill Cooling for the Electro-Magnetic Levitator in relation with Continuous Casting of steel
CEMEF	Centre de Mise en Forme des Matériaux
CFL	Courant–Friedrichs–Lewy
C.FL.	Computing and FLuids
CSF	Continuum Surface Force
DLR	Deutsches Zentrum für Luft- und Raumfahrt
DSPG	Darcy-Stabilising/Petrov-Galerkin
EML	Electromagnetic levitation
ESA	European Space Agency
FEM	Finite Element Method
FVM	Finite Volume Method
GMAW	Gas Metal Arc Welding
ISS	International Space Station
IWT	Institut für Werkstofftechnik
LHS	Left-hand side
LSIC	Least squares on incompressibility constraint
LSM	Level set method
MAC	Marker-and-cell
PF	Phase field
PSPG	Pressure-Stabilising/Petrov-Galerkin
RHS	Right-hand side
RF	Radiofrequency
RUB	Ruhr Universität Bochum
RVE	Representative Elementary Volume
SBB	Satisfying Babuška-Brezzi
SUPG	Streamline-Upwind/Petrov-Galerkin
VMS	Variational MultiScale
VOF	Volume Of Fluid

Contents

Chapter 1

Modelling Review

Contents

1.1 Modelling macrosegreation

Microsegregation models

Solid formation depends greatly on the ability of chemicals species to diffuse within each of the solid and liquid phases, but also across the solid-liquid interface. Furthermore, chemical diffusion like all other diffusional processes, is a time-dependent phenomenon. One can thus conclude that two factors influence the amount of solid formation: cooling rate and diffusion coefficients. However, convection and other mechanical mixing sources, homogenise the composition much faster than atomic diffusion.

Considering that $\langle D \rangle^l / \langle D \rangle^s \approx 10^3$-$10^4$ for species within the solidification interval, *complete mixing* in the liquid is often an acceptable assumption, regardless of the solidification time. Thus, we speak of infinite diffusion in the liquid. Diffusion in the solid, also known as *back diffusion*, is the only transport mechanism with very low diffusion coefficients. Therefore, chemical species require a long time, i.e. low cooling rate, to completely diffuse within the solid. The difference in diffusional behaviour at the scale of a secondary dendrite arm, is summarised by two limiting segregation models of perfect equilibrium and nonequilibrium, which are the lever rule and Gulliver-Scheil models, respectively. Afterwards, models with finite back diffusion are presented.

Lever rule

The lever rule approximation considers ideal equilibrium in and between all phases. It requires a long solidification time, i.e. extremely slow cooling rate, hence phase compositions are homogeneous ($w^{l^*} = w^l$ and $w^{s^*} = w^s$) at all times as a consequence of complete mixing. These compositions are given by:

$$w^l = w^{l^*} = k^{-1} w^{s^*} = k^{-1} w^s \tag{1.1}$$

$$w^s = w^{s^*} = \frac{k w_0}{k f^s + (1 - f^s)} \tag{1.2}$$

where w^l and w^s are the phase compositions and w^{l^*} and w^{s^*} are values at the solid-liquid interface in the liquid and solid phases, respectively. At the end of solidification, if a single solid phase forms, its composition is equal to the nominal composition, $w^s = w_0$.

Gulliver-Scheil

The other limiting case is the absence of diffusion in the solid or its limitation due to fast cooling. For a segregation coeffcicient less than unity, the consequence is a steady increase of the homogeneous liquid composition upon cooling while the solid composition continuously increases and becomes non-uniform. Compared to a full equilibrium approach, higher fractions of liquid will remain. In eutectic systems, liquid may exist until another solid structure forms, e.g. upon reaching the eutectic composition, triggering a eutectic solidification, that is the appearance of the lamellar eutectic microstructure. Assuming phase equilibrium is still valid, i.e. $w^{l*} = k^{-1}w^{s*}$, the phase compositions are given by:

$$w^l = w^{l*} = k^{-1}w^{s*} \tag{1.3}$$

$$w^{s*} = kw_0(1 - f^s)^{k-1} \tag{1.4}$$

$$w^s = \int_0^{f^s} w^{s*}\, \mathrm{d}f^s \tag{1.5}$$

Finite back diffusion

The assumption of a negligeable back diffusion overestimates the liquid composition and the resulting eutectic fraction. Therefore, many models studied the effect of limited diffusion in the solid. One of the earliest models is the Brody-Flemings models [Brody and Flemings 1966] that is a based on a differential solute balance equation for a parabolic growth rate, as follows:

$$w^l = w^{l*} = k^{-1}w^{s*} \tag{1.6}$$

$$w^{s*} = kw_0 \left[1 - (1 - 2\mathrm{Fo}^s k)\, f^s\right]^{\frac{k-1}{1-2\mathrm{Fo}^s k}} \tag{1.7}$$

where Fo^s is the dimensionless *Fourier number* for diffusion in the solid [Dantzig and Rappaz 2009]. It can be defined using the solid diffusion coefficient $\langle D \rangle^s$, solidification time t_s and the secondary dendrite arm spacing, λ_2, as follows:

$$\mathrm{Fo}^s = \frac{\langle D \rangle^s t_\mathrm{s}}{(\lambda_2/2)^2} \tag{1.8}$$

Several other models were since suggested and used. The interested reader is referred to the following non exhaustive list of publications: Clyne and Kurz [1981], Kobayashi [1988], Ni and Beckermann [1991], Wang and Beckermann [1993], Combeau et al. [1996], Martorano et al. [2003], and Tourret and Gandin [2009]. It is noted that some of these publications consider also a finite diffusion in the liquid phase. It also noted that

dealing with some aspects (e.g. multicomponent equilibrium phase diagrams, cross-diffusion of species, ...) is generally difficult and received a limited number of studies in the aim of determining a multicompponent segregation model, thus numerical approaches are favored.

1.1.1 Macroscopic solidification model: monodomain

In this section, we will present the macroscopic conservations equations that enable us to predict macrosegregation in single multiphase metal system.

Volume averaging

It is crucial for a solidification model to represent phenomena on the microscale, then scale up to predict macroscopic phenomena. Nevertheless, the characteristic length of a small scale in solidification may be represented by a dendrite arm spacing, for instance for the mushy zone permeability, as it may also be represented by an atomic distance if one is interested, for instance in the growth competition between diffusion and surface energy of the solid-liquid interface. Modelling infinitely small-scale phenomena could be prohibitively expensive in computation time, if we target industrial scales. Therefore, the common volume averaging approach alleviates these difficulties by making assumptions on intermediate scales. This technique allows bypassing this barrier by averaging small-scale variations on a so-called *representative volume element* (RVE) [Dantzig and Rappaz 2009] of volume V_E, with the following dimensional constraints: the element should be large enough to "see" and average microscopic fluctuations whilst being smaller than the scale of macroscopic variations.

Solid and liquid may exist simultaneously in the RVE, but we may also consider that no gas phase could be added (i.e. volume saturation with $V^s + V^l = V_E$). Moreover, temperature is generally assumed uniform and equal for all the phases. The formalism, introduced by Ni and Beckermann [1991], introduces a phase indicator function for any phase ϕ in the multiphase system:

$$\chi^\phi = \begin{cases} 1 & \text{in } \phi \\ 0 & \text{otherwise} \end{cases} \tag{1.9}$$

Then the approach suggests the following equations for any physical quantity ψ in system containing solid (s) and liquid (l) phases:

$$\langle \psi \rangle = \frac{1}{V_E} \int_{V_E} \psi \, \mathrm{d}\Omega = \langle \psi^s \rangle + \left\langle \psi^l \right\rangle \tag{1.10}$$

where $\langle\psi\rangle^s$ and $\langle\psi\rangle^l$ are phase averages of ψ. Then, for any phase ϕ, one can introduce the *phase intrinsic average* of ψ, denoted $\langle\psi\rangle^\phi$, by writing:

$$\left\langle\psi^\phi\right\rangle = \left\langle\chi^\phi\psi\right\rangle = \frac{1}{V_\mathrm{E}}\int_{V_\mathrm{E}}\chi^\phi\psi\,\mathrm{d}\Omega \tag{1.11a}$$

$$= \frac{1}{V_\mathrm{E}}\int_{V^\phi}\chi^\phi\psi\,\mathrm{d}\Omega \tag{1.11b}$$

$$= \frac{V^\phi}{V_\mathrm{E}}\left(\frac{1}{V^\phi}\int_{V^\phi}\chi^\phi\psi\,\mathrm{d}\Omega\right) \tag{1.11c}$$

$$= g^\phi\langle\psi\rangle^\phi \tag{1.11d}$$

where g^ϕ is the volume fraction of phase ϕ with $g^\phi = V_\phi/V_\mathrm{E}$. The transition from eq. (1.11a) to eq. (1.11b) is the consequence of eq. (1.9). To finalize, the averaging is applied to temporal and spatial derivation operators:

$$\left\langle\frac{\partial\psi}{\partial t}^\phi\right\rangle = \frac{\partial\left\langle\psi^\phi\right\rangle}{\partial t} - \int_{\Gamma^*}\psi^\phi\boldsymbol{v}^*\cdot\boldsymbol{n}^\phi\,\mathrm{d}A \tag{1.12}$$

$$\left\langle\boldsymbol{\nabla}\cdot\boldsymbol{\psi}^\phi\right\rangle = \boldsymbol{\nabla}\cdot\left\langle\boldsymbol{\psi}^\phi\right\rangle + \int_{\Gamma^*}\boldsymbol{\psi}^\phi\cdot\boldsymbol{n}^\phi\,\mathrm{d}A \tag{1.13}$$

where $\boldsymbol{v}^*$ is the local relative interface velocity and Γ^* is the solid-liquid interface, while n^ϕ is the normal to Γ^*, directed outwards. The surface integral terms in eqs. (1.12) and (1.13) are *interfacial averages* that express exchanges between the phases across the interface.

The previous equations will be used to derive a set of macroscopic conservation equations. It is noted that the intrinsic average $\langle\psi\rangle^\phi$ may be replaced by ψ^ϕ for notation simplicity, whenever the averaging technique applies. This notation is thus compatible with the previously introduced average defined for the solid composition when the latter is non-uniform eq. (1.5).

Macroscopic equations

A monodomain macroscopic model relies on four main conservation equations to predict macrosegregation in a single alloy where the latter is considered without any direct representation of interactions with another domain (moulds, air, ...). The general form of such a macroscopic conservation equation is given by:

$$\frac{\partial\psi}{\partial t} + \boldsymbol{\nabla}\cdot\psi\boldsymbol{v} + \boldsymbol{\nabla}\cdot\boldsymbol{j_\psi} = Q_\psi \tag{1.14}$$

where on the LHS, the first term is non-stationnary, the second term represents the convective transport of the quantity ψ while the third term is diffusive transport of ψ. The RHS term is a source term. To determine an general averaged macroscopic equation, we must write a phase-averaged conservation equation, for any volumetric physical quantity ψ:

$$\left\langle \frac{\partial \psi^\phi}{\partial t} \right\rangle + \left\langle \boldsymbol{\nabla} \cdot \psi^\phi \boldsymbol{v}^\phi \right\rangle + \left\langle \boldsymbol{\nabla} \cdot \boldsymbol{j}_{\psi^\phi} \right\rangle = \left\langle Q_{\psi^\phi} \right\rangle \tag{1.15}$$

The first LHS term in eq. (1.15) represents the time variation of ψ, the second term accounts for transport by advection while the third term accounts for diffusive transport of ψ, knowing its flux, $\boldsymbol{j}_\psi$. The RHS term represents a volumetric source. The considered equations are mass, energy, species conservation and momentum. The latter equation is written only for the liquid phase, as we assume a fixed and rigid solid phase ($\langle \boldsymbol{v} \rangle^s = \boldsymbol{0}$), thus the corresponding equation vanishes.

We may then write each averaged macroscopic conservation equation as the sum of local conservation equations for each phase in the RVE using the interfacial average terms previously defined in eqs. (1.12) and (1.13). For instance, if we replace ψ by ρ for each phase $\phi \in \{l, s\}$, eq. (1.15) gives two phase-averaged mass balances, with interfacial terms:

$$\frac{\partial}{\partial t}\left(g^l \langle \rho \rangle^l\right) + \boldsymbol{\nabla} \cdot \left(g^l \langle \rho \rangle^l \langle \boldsymbol{v} \rangle^l\right) = \int_{\Gamma_{l\text{-}s}} \langle \rho \rangle^l \boldsymbol{v}^{l*} \cdot \boldsymbol{n} \, \mathrm{d}A - \int_{\Gamma_{l\text{-}s}} \langle \rho \rangle^l \boldsymbol{v}^* \cdot \boldsymbol{n} \, \mathrm{d}A \tag{1.16a}$$

$$\frac{\partial}{\partial t}\left(g^s \langle \rho \rangle^s\right) + \boldsymbol{\nabla} \cdot \left(g^s \langle \rho \rangle^s \langle \boldsymbol{v} \rangle^s\right) = -\int_{\Gamma_{l\text{-}s}} \langle \rho \rangle^s \boldsymbol{v}^{s*} \cdot \boldsymbol{n} \, \mathrm{d}A + \int_{\Gamma_{l\text{-}s}} \langle \rho \rangle^s \boldsymbol{v}^* \cdot \boldsymbol{n} \, \mathrm{d}A \tag{1.16b}$$

where $\boldsymbol{v}^{l*}$ and $\boldsymbol{v}^{s*}$ are respectively, the liquid and solid phase velocity at the interface and $\boldsymbol{v}^*$ is the previously introduced solid-liquid interface velocity, while vector $\boldsymbol{n}$ is the the normal to the solid-liquid interface, with $\boldsymbol{n} = \boldsymbol{n}^s = -\boldsymbol{n}^l$.

Summing equations (1.16a) and (1.16b), results in the overall mass balance in the RVE:

$$\frac{\partial}{\partial t}\left(g^l \langle \rho \rangle^l + g^s \langle \rho \rangle^s\right) + \boldsymbol{\nabla} \cdot \left(g^l \langle \rho \rangle^l \langle \boldsymbol{v} \rangle^l + g^s \langle \rho \rangle^s \langle \boldsymbol{v} \rangle^s\right) =$$
$$\int_{\Gamma_{l\text{-}s}} \left(\langle \rho \rangle^l \boldsymbol{v}^{l*} - \langle \rho \rangle^s \boldsymbol{v}^{s*}\right) \cdot \boldsymbol{n} \, \mathrm{d}A - \int_{\Gamma_{l\text{-}s}} \left(\langle \rho \rangle^l - \langle \rho \rangle^s\right) \boldsymbol{v}^* \cdot \boldsymbol{n} \, \mathrm{d}A \tag{1.17}$$

where the RHS cancels to zero as shown by Ni and Beckermann [1991]. Moreover, the authors show that with their averaging technique, interfacial exchanges for energy, chemical species and momentum cancel out as they are equal in absolute value but opposite in sign. Regarding the LHS terms, their sum is defined along other variables

as follows:

$$\langle \rho \rangle = g^l \langle \rho \rangle^l + g^s \langle \rho \rangle^s \tag{1.18}$$

$$\langle \rho \boldsymbol{v} \rangle = g^l \langle \rho \rangle^l \langle \boldsymbol{v} \rangle^l + \underline{g^s \langle \rho \rangle^s \langle \boldsymbol{v} \rangle^s} \tag{1.19}$$

$$\langle \rho h \rangle = g^l \langle \rho \rangle^l \langle h \rangle^l + g^s \langle \rho \rangle^s \langle h \rangle^s \tag{1.20}$$

$$\langle \rho h \boldsymbol{v} \rangle = g^l \langle \rho \rangle^l \langle h \rangle^l \langle \boldsymbol{v} \rangle^l + \underline{g^s \langle \rho \rangle^s \langle h \rangle^s \langle \boldsymbol{v} \rangle^s} \tag{1.21}$$

$$\langle \rho w_i \rangle = g^l \langle \rho \rangle^l w_i^l + g^s \langle \rho \rangle^s w_i^s \tag{1.22}$$

$$\langle \rho w_i \boldsymbol{v} \rangle = g^l \langle \rho \rangle^l w_i^l \langle \boldsymbol{v} \rangle^l + \underline{g^s \langle \rho \rangle^s w_i^s \langle \boldsymbol{v} \rangle^s} \tag{1.23}$$

$$\left\langle \langle \rho \rangle^l \langle \boldsymbol{v} \rangle^l \right\rangle = \left\langle \langle \rho \rangle^l \langle \boldsymbol{v} \rangle^l \right\rangle^l = g^l \langle \rho \rangle^l \langle \boldsymbol{v} \rangle^l \tag{1.24}$$

$$\left\langle \langle \rho \rangle^l \langle \boldsymbol{v} \rangle^l \times \boldsymbol{v} \right\rangle = g^l \langle \rho \rangle^l \langle \boldsymbol{v} \rangle^l \times \langle \boldsymbol{v} \rangle^l + \underline{g^s \langle \rho \rangle^s \langle \boldsymbol{v} \rangle^l \times \langle \boldsymbol{v} \rangle^s} \tag{1.25}$$

The average diffusive fluxes are represented by $\langle \boldsymbol{q} \rangle$ for energy and $\langle \boldsymbol{j_i} \rangle$ for each solute species. They are respectively modelled using Fourier's thermal conduction law and Fick's first mass diffusion law:

$$\langle \boldsymbol{q} \rangle = -g^l \langle \kappa \rangle^l \boldsymbol{\nabla} T - g^s \langle \kappa \rangle^s \boldsymbol{\nabla} T = -\langle \kappa \rangle \boldsymbol{\nabla} T \tag{1.26}$$

$$\langle \boldsymbol{j_i} \rangle = -g^l \langle D \rangle^l \boldsymbol{\nabla} \left(\langle \rho \rangle^l w_i^l \right) - \underline{g^s \langle D \rangle^s \boldsymbol{\nabla} \left(\langle \rho \rangle^s w_i^s \right)} \tag{1.27}$$

In eq. (1.27), the macroscopic diffusion coefficient in the solid is neglected, by considering that for macroscopic scales, the average composition of the alloy is much more influenced by advective and diffusive transport in the liquid.

In eq. (1.26), we assume that phases are at thermal equilibrium, that is, temperature is uniform in the RVE. We also introduced the average thermal conductivity, $\langle \kappa \rangle$, defined as $\langle \kappa \rangle = g^s \langle \kappa \rangle^s + g^l \langle \kappa \rangle^l$.

Using eqs. (1.18) to (1.27) and following the same procedure done in eq. (1.17), the averaged equations for mass, energy and species conservation hence respectively write:

$$\frac{\partial \langle \rho \rangle}{\partial t} + \boldsymbol{\nabla} \cdot \langle \rho \boldsymbol{v} \rangle = 0 \tag{1.28}$$

$$\frac{\partial \langle \rho h \rangle}{\partial t} + \boldsymbol{\nabla} \cdot \langle \rho h \boldsymbol{v} \rangle - \boldsymbol{\nabla} \cdot (\langle \kappa \rangle \boldsymbol{\nabla} T) = 0 \tag{1.29}$$

$$\frac{\partial \langle \rho w_i \rangle}{\partial t} + \boldsymbol{\nabla} \cdot \langle \rho w_i \boldsymbol{v} \rangle - \boldsymbol{\nabla} \cdot \left(g^l \langle D \rangle^l \boldsymbol{\nabla} \left(\langle \rho \rangle^l w_i^l \right) \right) = 0 \tag{1.30}$$

As stated previously, the momentum balance in the solid phase is not taken into consideration, hence we do not sum the corresponding conservation equations. This has consequences on the advection terms in energy and species conservation, and later on we will show the consequences on the momentum conservation in the liquid.

First, the advection terms in eqs. (1.29) and (1.30) shall be redefined by considering that the fluid is incompressible $(\boldsymbol{\nabla} \cdot \langle \boldsymbol{v^l} \rangle = 0)$, which yields:

$$\boldsymbol{\nabla} \cdot \langle \rho \boldsymbol{v} \rangle = \left\langle \boldsymbol{v^l} \right\rangle \cdot \boldsymbol{\nabla} \left(\langle \rho \rangle^l \right) \tag{1.31}$$

$$\boldsymbol{\nabla} \cdot \langle \rho h \boldsymbol{v} \rangle = \left\langle \boldsymbol{v^l} \right\rangle \cdot \boldsymbol{\nabla} \left(\langle \rho \rangle^l \langle h \rangle^l \right) \tag{1.32}$$

$$\boldsymbol{\nabla} \cdot \langle \rho w_i \boldsymbol{v} \rangle = \left\langle \boldsymbol{v^l} \right\rangle \cdot \boldsymbol{\nabla} \left(\langle \rho \rangle^l \, w_i^l \right) \tag{1.33}$$

As for the liquid momentum balance, we write:

$$\frac{\partial}{\partial t} \left(\langle \rho \rangle^l \, g^l \langle \boldsymbol{v} \rangle^l \right) + \boldsymbol{\nabla} \cdot \left(\langle \rho \rangle^l \, g^l \langle \boldsymbol{v} \rangle^l \times \langle \boldsymbol{v} \rangle^l \right) = \boldsymbol{\nabla} \cdot \left(g^l \overline{\overline{\boldsymbol{\sigma^l}}} \right) + g^l \boldsymbol{F}_{\mathrm{v}}^l + \boldsymbol{\Gamma}^l \tag{1.34}$$

where $\boldsymbol{F}_{\mathrm{v}}^l$ is the vector of external body forces exerted on the liquid phase. In our case, it accounts for the fluid's weight:

$$\boldsymbol{F}_{\mathrm{v}}^l = \langle \rho \rangle^l \, \mathbf{g} \tag{1.35}$$

The interfacial momentum transfer between the solid and liquid phases in eq. (1.34) is modelled by a momentum flux vector $\boldsymbol{\Gamma}^l$, consisting of hydrostatic and deviatoric parts, such that:

$$\boldsymbol{\Gamma}^l = \boldsymbol{\Gamma}_p^l + \boldsymbol{\Gamma}_{\mathbb{S}}^l \tag{1.36}$$

$$\boldsymbol{\Gamma}_p^l = p^{l*} \boldsymbol{\nabla} g^l = p^l \boldsymbol{\nabla} g^l \tag{1.37}$$

$$\boldsymbol{\Gamma}_{\mathbb{S}}^l = -g^{l^2} \mu^l \mathbb{K}^{-1} \left(\langle \boldsymbol{v} \rangle^l - \langle \boldsymbol{v} \rangle^s \right) \tag{1.38}$$

where p^{l*} is the pressure at the interface, considered to be equal to the liquid hydrostatic pressure p^l, $\mathbb{K}$ is a permeability scalar (isotropic) computed using **??** and μ^l is the liquid's dynamic viscosity. The general form of the Cauchy liquid stress tensor in eq. (1.34) is decomposed as follows:

$$\left\langle \overline{\overline{\boldsymbol{\sigma^l}}} \right\rangle = g^l \overline{\overline{\boldsymbol{\sigma^l}}} = - \left(\left\langle p^l \right\rangle - \lambda \boldsymbol{\nabla} \cdot \left\langle \boldsymbol{v^l} \right\rangle \right) \overline{\overline{\mathbf{I}}} + \left\langle \overline{\overline{\mathbb{S}}}^l \right\rangle \tag{1.39}$$

where λ is a dilatational viscosity [Dantzig and Rappaz 2009] and $\overline{\overline{\mathbb{S}}}^l$ is the liquid strain deviator tensor.

In the literature, the coefficient λ is taken proportional to the viscosity: $\lambda = \frac{2}{3} \mu^l$. However, as we consider an incompressible flow, the divergence term vanishes, thus rewrit-

ing eq. (1.39) as follows:

$$\left\langle \overline{\overline{\boldsymbol{\sigma}^l}} \right\rangle = -\left\langle p^l \right\rangle \overline{\overline{\mathbf{I}}} + \left\langle \overline{\overline{\mathbb{S}}}^l \right\rangle \tag{1.40a}$$

$$\left\langle \overline{\overline{\boldsymbol{\sigma}^l}} \right\rangle = -\left\langle p^l \right\rangle \overline{\overline{\mathbf{I}}} + 2\mu^l \left\langle \overline{\overline{\dot{\varepsilon}^l}} \right\rangle \tag{1.40b}$$

where the transition from eq. (1.40a) to eq. (1.40b) is made possible by assuming a Newtonian behaviour for the liquid phase. The strain rate tensor, $\left\langle \overline{\overline{\dot{\varepsilon}^l}} \right\rangle$, depends on the average liquid velocity:

$$\left\langle \overline{\overline{\dot{\varepsilon}^l}} \right\rangle = \frac{1}{2}\left(\overline{\overline{\boldsymbol{\nabla}}} \left\langle \boldsymbol{v^l} \right\rangle + \overline{\overline{\boldsymbol{\nabla}^{\mathrm{t}}}} \left\langle \boldsymbol{v^l} \right\rangle \right) \tag{1.41}$$

Finally, we obtain the final form of momentum conservation in the liquid phase coupled with the averaged mass balance, by injecting eqs. (1.35), (1.37), (1.38), (1.40b) and (1.41) in eq. (1.34):

$$\frac{\partial}{\partial t}\left(\langle\rho\rangle^l \left\langle \boldsymbol{v^l} \right\rangle \right) + \frac{1}{g^l}\boldsymbol{\nabla}\cdot\left(\langle\rho\rangle^l \left\langle \boldsymbol{v^l} \right\rangle \times \left\langle \boldsymbol{v^l} \right\rangle \right) = $$
$$-g^l\boldsymbol{\nabla}p^l - \mu^l\boldsymbol{\nabla}\cdot\left(\overline{\overline{\boldsymbol{\nabla}}} \left\langle \boldsymbol{v^l} \right\rangle + \overline{\overline{\boldsymbol{\nabla}^{\mathrm{t}}}} \left\langle \boldsymbol{v^l} \right\rangle \right) - g^l\mu^l\mathbb{K}^{-1} \left\langle \boldsymbol{v^l} \right\rangle + g^l \langle\rho\rangle^l \mathbf{g} \tag{1.42}$$

where we intentionally employed the *superficial velocity*, $\left\langle \boldsymbol{v^l} \right\rangle = g^l\langle\boldsymbol{v}\rangle^{\boldsymbol{l}}$, as the main unknown, together with the liquid pressure p^l. This system, when modelled in 3D, has a total of 4 unknowns (velocity vector and pressure) and 3 equations (X,Y and Z projections for the velocity vector). A fourth equation provided by the mass balance (eq. (1.28))is therefore added for closure, giving the following system of equations :

$$\begin{cases} \dfrac{\partial}{\partial t}\left(\langle\rho\rangle^l \left\langle \boldsymbol{v^l} \right\rangle \right) + \dfrac{1}{g^l}\boldsymbol{\nabla}\cdot\left(\langle\rho\rangle^l \left\langle \boldsymbol{v^l} \right\rangle \times \left\langle \boldsymbol{v^l} \right\rangle \right) = \\ \quad -g^l\boldsymbol{\nabla}p^l - \mu^l\boldsymbol{\nabla}\cdot\left(\overline{\overline{\boldsymbol{\nabla}}} \left\langle \boldsymbol{v^l} \right\rangle + \overline{\overline{\boldsymbol{\nabla}^{\mathrm{t}}}} \left\langle \boldsymbol{v^l} \right\rangle \right) - g^l\mu^l\mathbb{K}^{-1} \left\langle \boldsymbol{v^l} \right\rangle + g^l \langle\rho\rangle^l \mathbf{g} \\[2mm] \boldsymbol{\nabla}\cdot\left\langle \boldsymbol{v^l} \right\rangle = 0 \end{cases} \tag{1.43}$$

Last, the Boussinesq approximation allows taking a constant density in the inertial terms of eq. (1.43) while the variations responsible for buoyancy forces can be deduced from temperature and liquid concentration using thermodynamic databases or directly using known thermal and solutal expansion coefficients, respectively β_T and $\beta_{w_i^l}$, and the reference density value ρ_0^l:

$$\langle \rho \rangle^l = \rho_0^l \left(1 - \beta_T \left(T - T_0 \right) - \sum_i \beta_{w_i^l} \left(w_i^l - \langle w_i \rangle_0^l \right) \right) \qquad (1.44)$$

Hence, the final set of equations is better known as the incompressible *Navier-Stokes* equations, applied to a solidifying melt:

$$
\begin{cases}
\rho_0^l \left(\dfrac{\partial \langle \boldsymbol{v}^l \rangle}{\partial t} + \dfrac{1}{g^l} \boldsymbol{\nabla} \cdot \left(\langle \boldsymbol{v}^l \rangle \times \langle \boldsymbol{v}^l \rangle \right) \right) = \\[2mm]
\quad - g^l \boldsymbol{\nabla} p^l - \mu^l \boldsymbol{\nabla} \cdot \left(\overline{\overline{\boldsymbol{\nabla}}} \langle \boldsymbol{v}^l \rangle + \overline{\overline{\boldsymbol{\nabla}^t}} \langle \boldsymbol{v}^l \rangle \right) - g^l \mu^l \mathbb{K}^{-1} \langle \boldsymbol{v}^l \rangle + g^l \langle \rho \rangle^l \, \mathbf{g} \\[4mm]
\boldsymbol{\nabla} \cdot \langle \boldsymbol{v}^l \rangle = 0
\end{cases}
\qquad (1.45)
$$

Since all conservation equations were presented and simplified by the main assumption of a static solid phase, we may include them in a graphical summary in section 1.1.1

1.2 Eulerian and Lagrangian motion description

1.2.1 Overview

In mechanics, it is possible to describe motion using two well-known descriptions: Eulerian and Lagrangian. To start with the latter, it describes the motion of a particle by attributing a reference frame that moves with the particle. In other words, the particle itself is the center of a reference frame moving at the same speed during time. The position vector, denoted by $\boldsymbol{x}$, is hence updated as follows:

$$\boldsymbol{x}^{(t+1)} = \boldsymbol{x}^{(t)} + \boldsymbol{v} \Delta t \qquad (1.49)$$

As such, the total variation of any physical quantity ψ related to the particle can be found by deriving with respect to time, $\frac{\mathrm{d}\psi}{\mathrm{d}t}$. In contrast to the Lagrangian description, the Eulerian description considers a fixed reference frame and independent of the particle's trajectory. The total variation of ψ cannot be simply described by a temporal derivative, since the particle's velocity is not known to the reference frame, and thus the velocity effect, namely the advective transport of ψ, should also be considered as

Conservation of energy (Nonlinear Heat Transfer)

$$\frac{\partial \langle \rho h \rangle}{\partial t} + \left\langle \boldsymbol{v^l} \right\rangle \cdot \boldsymbol{\nabla} \left(\langle \rho \rangle^l \langle h \rangle^l \right) - \boldsymbol{\nabla} \cdot \left(\langle \kappa \rangle \boldsymbol{\nabla} T \right) = 0 \qquad (1.46)$$

T^t

Microsegregation

Full thermodynamic mapping:

Phase fraction	$(T, \langle w_i \rangle) \to g^\phi$
Phase composition	$(T, \langle w_i \rangle) \to \langle w_i \rangle^\phi$
Phase enthalpy	$(T, \langle w_i \rangle^\phi) \to \langle h \rangle^\phi$

Segregation model (SM) + partial thermodynamic mapping:

Phase fraction/composition	$(T, \langle w_i \rangle) \xrightarrow{\text{SM}} (g^\phi, \langle w_i \rangle^\phi)$
Enthalpy mapping	$(T, \langle w_i \rangle^\phi) \to \langle h \rangle^\phi$

$\langle \rho h \rangle^t$

No — Convergence

Conservation of chemical species (Macrosegregation)

$$\frac{\partial \langle \rho w_i \rangle}{\partial t} + \left\langle \boldsymbol{v^l} \right\rangle \cdot \boldsymbol{\nabla} \left(\langle \rho \rangle^l w_i^l \right) - \boldsymbol{\nabla} \cdot \left(g^l \langle \rho \rangle^l \langle D \rangle^l \boldsymbol{\nabla} w_i^l \right) = 0 \quad (1.47)$$

$\langle \rho w_i \rangle^t$

Conservation of liquid momentum (Navier-Stokes)

$$\begin{cases} \rho_0^l \left(\dfrac{\partial \langle \boldsymbol{v^l} \rangle}{\partial t} + \dfrac{1}{g^l} \boldsymbol{\nabla} \cdot \left(\langle \boldsymbol{v^l} \rangle \times \langle \boldsymbol{v^l} \rangle \right) \right) = \\[2mm] \quad - g^l \boldsymbol{\nabla} p^l - 2\mu^l \boldsymbol{\nabla} \cdot \left(\overline{\overline{\boldsymbol{\nabla}}} \langle \boldsymbol{v^l} \rangle + \overline{\overline{\boldsymbol{\nabla}^{\mathsf{t}}}} \langle \boldsymbol{v^l} \rangle \right) - g^l \mu^l \mathbb{K}^{-1} \langle \boldsymbol{v^l} \rangle + g^l \langle \rho \rangle^l \mathbf{g} \\[3mm] \boldsymbol{\nabla} \cdot \langle \boldsymbol{v^l} \rangle = 0 \end{cases}$$

$\left\langle \boldsymbol{v^l} \right\rangle^t, (p^l)^t$

$$(1.48)$$

Fig. 1.1 – Graphical resolution algorithm of the conservation equations used in a monodomain macroscopic model to predict macrosegregation for a time inrement t. The blue boxes represent the output of each equation.

follows:

$$\frac{\mathrm{D}\psi}{\mathrm{D}t} = \frac{\partial \psi}{\partial t} + \underbrace{\boldsymbol{v} \cdot \boldsymbol{\nabla}\psi}_{\substack{\text{Advective} \\ \text{Transport}}} \qquad (1.50)$$

In this case, the LHS term is also known as *total* or *material derivative*. The importance of these motion descriptions is essential to solve mechanics, whether for fluids or solids, using a numerical method like the finite element method (FEM). One of the main steps of this method is to spatially discretise a continuum into a grid of points (nodes, vertices ...), where any physical field shall be accordingly discretised. Now, if we focus on a node where velocity has a non zero value and following the previously made analysis, two outcomes are possible: either the node would be fixed (Eulerian) or it would move by a distance proportional to the prescribed velocity (Lagrangian). In the latter case, points located on the boundaries constantly require an update of the imposed boundary conditions.

From these explanations, one can deduce that an Eulerian framework is suited for fluid mechanics problems where velocities are high and may distort the mesh points, whereas the Lagrangian framework is better suited for solid mechanics problems where deformation velocities are relatively low and should well behave when predicting strains.

Another motion description has emerged some decades ago, Hirt [1971] call it the Arbitrary Langrangian-Eulerian (ALE) method. ALE combines advantages from both previous descriptions as it dictates a Lagrangian behaviour at "solid" nodes where solid is deforming, and an Eulerian behaviour at "fluid" nodes.

1.2.2   Interface capturing

As no solid deformation is considered in this work, the Eulerian framework is a convenient choice. Solidification shrinkage is to be considered in our current scope, so it will deform the alloy's outer surface in contact with the air. We intend to track this interface and its motion over time via a numerical method. A wide variety of methods accomplish this task while they yield different advantages and disadvantages.

Such methods fall into two main classes, either interface tracking or interface capturing, among which we cite: marker-and-cell (MAC) [Harlow and Welch 1965], volume of fluid (VOF) [Hirt and Nichols 1981], phase field methods (PF) [Karma and Rappel 1996; Beckermann et al. 1999], level set method (LSM) [Osher and Sethian 1988], coupled level set - VOF method and others. The interested reader may refer to quick references by Prosperetti [2002] and Maitre [2006] about these methods.

In the past years, the level set method received a considerable attention in many computational fields. For this reason, we will focus on this method henceforth, giving a brief literature review and technical details in the next sections.

1.3 Solidification models with level set

In classic solidification problems, the need to track an interface occurs usually at the solid-liquid interface, that is why the phase field method [Karma and Rappel 1996; Boettinger et al. 2002] and the level set method [Chen et al. 1997; Gibou et al. 2003; Tan and Zabaras 2007] were applied at a microscale to follow mainly the dendritic growth of a single solid crystal in an undercooled melt. In our case however, when we mention "solidification models using LSM", we do not mean the solid-liquid interface inside the alloy, but it is the alloy(liquid)-air interface that we intend to track, assuming that microscale phenomena between the phases within the alloy, are averaged using the previously defined technique in section 1.1.1.

Very few models were found in the literature, combining solidification and level set as stated previously. Du et al. [2001] applied it to track the interface between two molten alloys in a double casting technique. Welding research, on another hand, has been more active adapting the level set methodology to corresponding applications. Two recent works used the metal-air level set methodology in welding simulations and showed promising results: Desmaison et al. [2014] employed this methodolody to simulate a hybrid arc and laser beam welding used in high thickness steel sheet welding, then later, Chen [2014] applied it to gas metal arc welding (GMAW) to predict the solidification grain structure of remelted zones. More recently, Courtois et al. [2014] used the same methodology but this time to predict keyhole defect formation in spot laser welding. The tracked interface in this case was that between the molten alloy and the corresponding vapor phase.

1.4 The level set method

Firstly introduced by Osher and Sethian [1988], this method became very popular in studying multiphase flows. It is reminded that the term *multiphase* in computational domains usually refers to multiple fluids, and thus should not be mixed with definition of a phase in the current solidification context. For disambiguation, we shall use *multifluid flow* when needed.

The great advantage lies in the way the interface between two fluids, F_1 and F_2 is implicitly captured, unlike other methods where the exact interface position is needed.

In a discrete domain, the concept is to assign for each mesh node of position vector x, the minimum distance $d_\Gamma(x)$ separating it from an interface Γ. The distance function, denoted α and defined in eq. (1.51), is then signed positive or negative, based on the fluid or domain to which the node belongs.

$$\alpha(x) = \begin{cases} d_\Gamma(x) & \text{if } x \in F_1 \\ -d_\Gamma(x) & \text{if } x \in F_2 \\ 0 & \text{if } x \in \Gamma \end{cases} \tag{1.51}$$
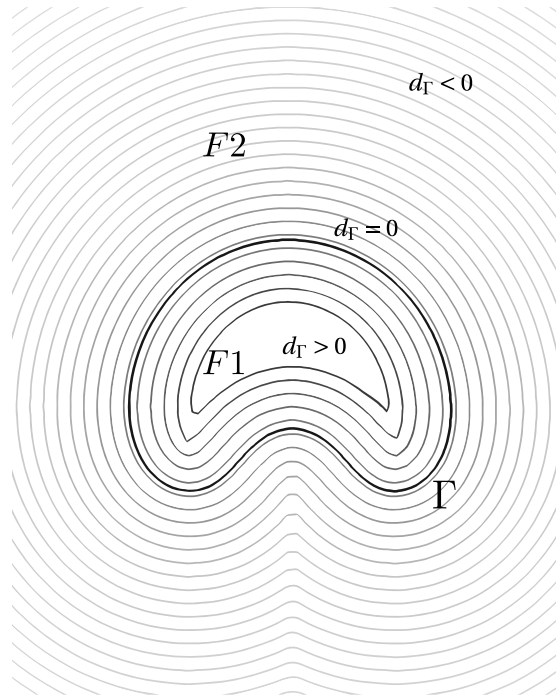
Fig. 1.2 – Schematic of the interface Γ (thick black line) of a rising air bubble (F_1) in water (F_2). The other contours represent isovalues of the distance function around and inside the interface contour. Those outside are signed negative whereas inside they are signed positive.

1.4.1   Diffuse interface

The level set has many attractive properties that allows seamless implementation in 2D and 3D models. It is a continuously differentiable C^1-function. The Heaviside function is also continuous but non differentiable, with an abrupt transition from 0 to

1 across the sharp interface, as follows:

$$H = H\left(\alpha\left(\boldsymbol{x}\right)\right) = \begin{cases} 0 & \text{if } \alpha\left(\boldsymbol{x}\right) < 0 \\ 1 & \text{if } \alpha\left(\boldsymbol{x}\right) \geqslant 0 \end{cases} \tag{1.52}$$

With the help of eq. (1.52), we can define the geometric "presence" of a domain with respect to the interface. As such, material properties depend upon this function, which will be discussed later in section 1.4.2. It is established that a steep transition can lead to numerical problems, so the Heaviside function should be smoothed in a volume of fixed thickness around the interface.

Sinusoidal smoothing in eq. (1.53) is widely used with level set formulations.

$$H = \begin{cases} 0 & \text{if } \alpha\left(\boldsymbol{x}\right) < -\varepsilon \\ 1 & \text{if } \alpha\left(\boldsymbol{x}\right) > \varepsilon \\ \frac{1}{2}\left(1 + \frac{\alpha(\boldsymbol{x})}{\varepsilon} + \frac{1}{\pi}\sin\left(\frac{\pi\alpha(\boldsymbol{x})}{\varepsilon}\right)\right) & \text{if } -\varepsilon \leq \alpha\left(\boldsymbol{x}\right) \leq \varepsilon \end{cases} \tag{1.53}$$

where the interval $[-\varepsilon; +\varepsilon]$ is an artificial interface thickness around the zero distance.

Defining a diffuse interface rather than a sharp one, is also a common approach in phase field methods [Beckermann et al. 1999; Sun and Beckermann 2004]. It is emphasized that the latter methods give physically meaningful analysis of a diffuse interface and the optimal thickness by thoroughly studying the intricate phenomena happening at the scale of the interface. However, for level set methods, there has not been a formal work leading the same type of analysis. For this reason, many aspects of the level set method lack physical meanings but remain computationally useful. In a recent paper by Gada and Sharma [2009], the authors respond partially to this problem by analysing and deriving conservation equations using a level set in a more meaningful way, but do not discuss the diffuse interface aspect.

The Dirac delta function is also an important property to convert surface integrals to volume terms, which could turn useful when modelling surface tension effects for instance, using the *continuum surface force* method (CSF) [Brackbill et al. 1992]. A smooth Dirac function, plotted in fig. 1.3 along with the smooth Heaviside function within an interface thickness of $[-\varepsilon; +\varepsilon]$, is derived from the Heaviside as follows:

$$\delta\left(\alpha\right) = \delta\left(\alpha\left(\boldsymbol{x}\right)\right) = \frac{\partial H}{\partial\alpha\left(\boldsymbol{x}\right)} = \begin{cases} \frac{1}{2\varepsilon}\left(1 + \cos\left(\frac{\pi\alpha(\boldsymbol{x})}{\varepsilon}\right)\right) & \text{if } |\alpha\left(\boldsymbol{x}\right)| \leqslant \varepsilon \\ 0 & \text{if } |\alpha\left(\boldsymbol{x}\right)| > \varepsilon \end{cases} \tag{1.54}$$

The Heaviside and delta Dirac functions can be readily processed to obtain other

geometric properties from the level set, which are extremely useful. In the context of a system Ω, containing two domains metal (M) and gas (G) seperated by an interface Γ, the following properties are interesting to study [Peng et al. 1999]:

$$\text{normal vector}: \boldsymbol{n} = \frac{\boldsymbol{\nabla}\alpha}{\|\boldsymbol{\nabla}\alpha\|} \tag{1.55}$$

$$\text{curvature}: \zeta = -\boldsymbol{\nabla} \cdot \boldsymbol{n} \tag{1.56}$$

$$\text{surface area of the air-metal interface}: A^{\Gamma} = \int_{\Omega} \delta\left(\alpha\right)\|\boldsymbol{\nabla}\alpha\|\,\mathrm{d}\Omega \tag{1.57}$$

$$\text{metal volume}: V^{M} = \int_{\Omega} H^{M}\,\mathrm{d}\Omega \tag{1.58}$$

It is reminded that for a 2D case, eq. (1.57) evaluates a length instead of the area while eq. (1.58) gives the area instead of volume. Finally, within the diffuse interface, fluids properties may vary linearly or not, depending on the mixing law, which is presented in the next section.
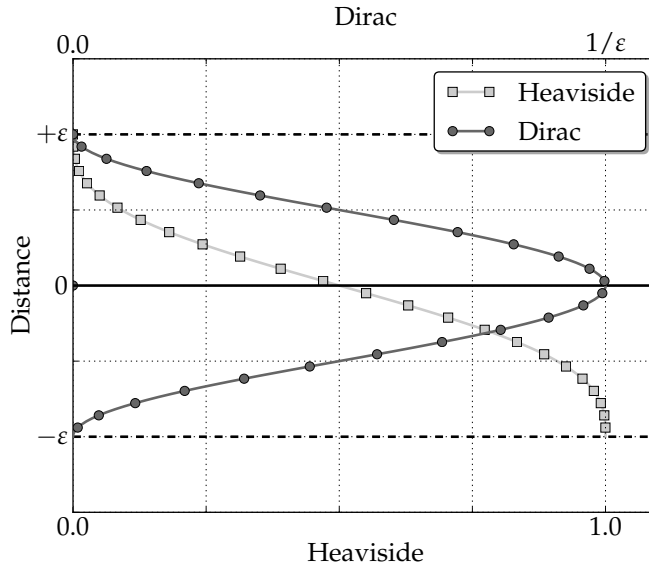
Fig. 1.3 – Schematic of two level properties inside the diffuse interface: Heaviside (lower x-axis) and Dirac delta (upper x-axis) functions. Note that the peak of the Dirac function depends on the interface thickness to ensure a unity integral of the delta function over Ω.

1.4.2 Mixing Laws

A *monolithic* resolution style, as opposed to a *partitioned* resolution, is based on solving a single set of equations for both fluids separated by an interface, as if a single fluid were considered. Level set is one among many methods that use the monolithic

style to derive a single set of conservation equations for both fluids. The switch from one material to the other is implicitly taken care of by using the Heaviside function as well as mixing laws. These laws are crucial to define how properties vary across the diffuse interface in view of a more accurate resolution. The most frequently used mixing law in the literature is the arithmetic law. Other transitions are less known such as the harmonic and logarithmic mixing. The first law is maybe the most intuitive and most used for properties mixture as it emanates from VOF-based methods. If we consider any property ψ (for instance the fluid's dynamic viscosity μ) then the arithmetic law will give a mixed property $\widehat{\psi}$ as follows:

$$\widehat{\psi} = H^{F_1}\psi^{F_1} + H^{F_2}\psi^{F_2} \tag{1.59}$$

Basically, the result is an average property that follows the same trend as the Heaviside function. As for the harmonic law, it writes:

$$\widehat{\psi} = \left(\frac{H^{F_1}}{\psi^{F_1}} + \frac{H^{F_2}}{\psi^{F_2}}\right)^{-1} \tag{1.60}$$

and last, the logarithmic law writes:

$$\widehat{\psi} = n^{\left(H^{F_1}\log_n \psi^{F_1} + H^{F_2}\log_n \psi^{F_2}\right)} \tag{1.61}$$

where n is any real number serving as a logarithm base, which often is either the exponential e or 10.

The mixture result with this law is the same, regardless of the value of n. By looking to fig. 1.4, we clearly see that the difference between all three approaches is the property weight given to each side of the level set in the mixture. The arithmetic law, being symmetric, has equal weights, ψ^{F_1} and ψ^{F_2}, in the final mixture. Nevertheless, the asymmetric harmonic mixing varies inside the diffuse interface with a dominant weight of one property over the other. As for the logarithmic mixture, it can be seen as an intermediate transition between the preceding laws.

As long as the interface thickness is small enough, the choice of a mixing law should not drastically change the result, inasmuch as it depends on the discretisation resolution of the interface. This fact made the arithmetic mixing the most applied one, because it is symmetric and easy to implement (no handling of potential division problems like harmonic laws for instance). However, Strotos et al. [2008] claim that the harmonic law proves to conserve better diffusive fluxes at the interface. More recently, an interesting study made by Ettrich et al. [2014] focused on mixing thermal properties using a phase field method. They define a diffuse interface in which they separately
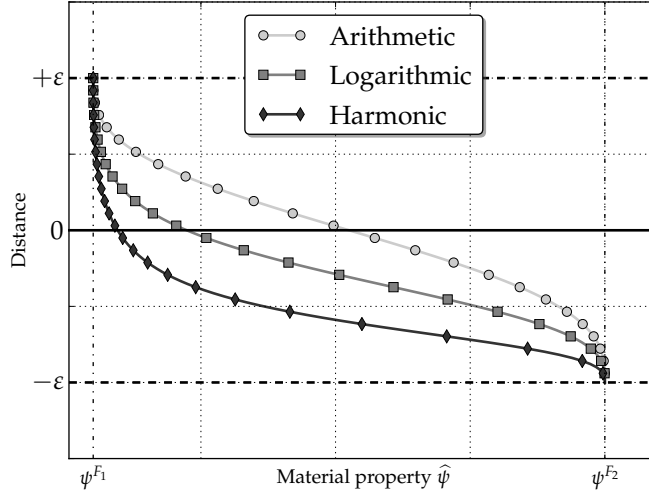
Fig. 1.4 – Three mixing laws, arithmetic, logarithmic and harmonic commonly used in monolithic formulations.

mix the thermal conductivity, κ, and the heat capacity, C_p, then compute the thermal diffusivity as the ratio of these properties. Later, the authors compare the temperature field obtained by diffusion to a reference case in order to decide which combination of mixing laws gives the best result. Despite not being directly related to a level set method, this work gives an insight of the mixing laws possibilities and their effect on pure thermal diffusion. Otherwise, little work has been found in the literature on the broad effects of mixture types on simulation results in a level set context.

1.5 Interface motion

When a physical interface needs to have topology changes because of fluid structure interaction or surface tension for instance, the level set model can follow these changes by a transport step. The idea is to advect the signed distance function, its zero isovalue representing the interface and all other distant isovalues, with velocity field as input. The motion of the interface is thus expressed by:

$$\frac{d\alpha}{dt} = \frac{\partial \alpha}{\partial t} + \boldsymbol{v} \cdot \boldsymbol{\nabla}\alpha = 0 \tag{1.62}$$

1.5.1 Level set transport

The finite element method gives the fully discretised weak form of eq. (1.62) by using a convenient set of test functions α^* belonging the Hilbertian Sobolev space:

$$\int_\Omega \alpha^* \frac{\partial \alpha}{\partial t} \, \mathrm{d}\Omega + \int_\Omega \alpha^* \boldsymbol{v} \cdot \boldsymbol{\nabla} \alpha \, \mathrm{d}\Omega = 0 \qquad \forall \alpha^* \in \mathcal{H}^1 (\Omega) \tag{1.63}$$

The spatial discretisation of α assigns, for each of the total N nodes of a simplex, the following values:

$$\alpha = \sum_N P_j \alpha_j \tag{1.64}$$

Furthermore, with the standard Galerkin method, we replace test functions by the interpolation functions P_j, then we apply a temporal discretisation for the main unknowns by a forward (implicit) finite difference in time. Consequently, eq. (1.63) can be recast as follows:

$i, j : 1 \to \text{Nnodes}$

$$\frac{1}{\Delta t} \left(\alpha_j^t - \alpha_j^{t-\Delta t} \right) \int_\Omega P_i P_j \, \mathrm{d}\Omega + \alpha_j^t \int_\Omega \boldsymbol{v^t} \cdot \boldsymbol{\nabla} P_j \, \mathrm{d}\Omega = 0 \tag{1.65a}$$

$$\left[\frac{1}{\Delta t} \int_\Omega P_i P_j \, \mathrm{d}\Omega + \int_\Omega \boldsymbol{v^t} \cdot \boldsymbol{\nabla} P_j \, \mathrm{d}\Omega \right] \alpha_j^t = \frac{1}{\Delta t} \int_\Omega \alpha^{t-\Delta t} P_i \, \mathrm{d}\Omega \tag{1.65b}$$

$$\left[\mathcal{M}_{ij} + \mathcal{A}_{ij} \right] \alpha_j^t = \mathcal{F}_i \tag{1.65c}$$

where $\mathcal{M}_{ij}$ and $\mathcal{A}_{ij}$ are respectively the mass (or capacity) matrix and advection matrix, both written within a local finite element, whereas $\mathcal{F}_i$ is a local vector of known quantities from the previous time step. The solution of the linear system in eq. (1.65c) is the transported distance function.

When the convection regime becomes more dominant than diffusion (for high Peclet number), the standard Galerkin method may lead to instabilities in the solution. In this case, stabilisation is crucial to avoid these oscillations, unless very fine remeshing is done "such that convection no longer dominates on an element level", as stated by Brooks and Hughes [1982]. The authors give a brief explanation of how numerically a convection-dominated equation can lead to oscillatory solutions with the standard Galerkin approximation. They proposed a stabilisation scheme, the Streamline Upwind Petrov-Galerkin, better known as SUPG, to stabilise advection dominated Navier-Stokes equations. However, their technique applies to any convection-diffusion equation. The SUPG method consists of modifying the test functions (like a classical Petrov-

Galerkin method) by adding artificial diffusion in the flow direction. The modified test function writes:

$$\alpha^*_{SUPG} = \alpha^* + \underbrace{C^E_{SUPG} \left(\boldsymbol{v}_{\text{transport}} \cdot \boldsymbol{\nabla}\alpha^* \right)}_{\text{Upwind contribution}} \tag{1.66}$$

where the upwind contribution for each finite element E depends on a stabilisation parameter C^E_{SUPG} that is expressed as follows:

$$C^E_{SUPG} = \frac{h^E}{v^E_{\text{flow}}} \tag{1.67}$$

Equation (1.67) shows that the SUPG parameter represents a time constant relative to an element mesh size, h^E, and an average velocity that should represent the magnitude in the flow direction. In the present work, all convection-diffusion equations are stabilised with the SUPG method, namely the conservation of mass, energy, momentum and chemical species as well as the level set transport.

1.5.2 Level set regularisation

Upon transport the distance function field, a crucial property of the level set may be partially or totally lost over the domain, which is:

$$\begin{cases} \|\boldsymbol{\nabla}\alpha\| = 1 \\ \alpha(x,t) = 0 \qquad \text{if } x \in \Gamma(t) \end{cases} \tag{1.68}$$

The closer this L^2-norm to one, the more regular the level set. An irregular distance function induces cumulative numerical errors while transporting distance values far from the interface, resulting in wrong distance information, and loss of properties that make up a "distance function". To show one the benefit of level set regularisation, Basset [2006] states after showing several tests of distance function transport, that regularised distance functions transported with a standard Galerkin method (i.e. without any stabilisation) show better "quality" globally in the domain, compared to initially non-regularised ones. When the transport equation in eq. (1.62) is discretised in time then solved, a *regularisation* (also known as *reinitialisation*) is necessary to conserve as much as possible the property in eq. (1.68).
Figure 1.5 shows the need of regularisation in two different simulations of the same phenomenon: rising air bubble inside water. The importance of this well studied case [Sussman et al. 1994; Hysing et al. 2009] is that the interface between two fluids is

highly deformable as the bubble rises because of buoyancy, and therefore the task of tracking the dynamic interface while maintaining an accurate distance function is a considerable numerical task. In the first simulation, the distance contours are squeezed against the zero-distance contour marked by the thick black line. A closer look to the interface reveals undesired distortions, with a "wavy" shape at some points. This effect is evidently an artefact of a level set transport lacking subsequent reinitialisation, inasmuch as the surface tension tends to minimise the total surface area and make it as smooth as possible. Nevertheless, the second simulation unveils much better results, especially how the interface shows no sign of destabilisation. We also note the regular spacing between contours, which is a consequence of conserving the property defined in eq. (1.68). This improvement is attributed to the regularization done at each time step after the transport. In the forthcoming sections, we present three regularisation methods, then show their strong and weak points.

(a)   (b)
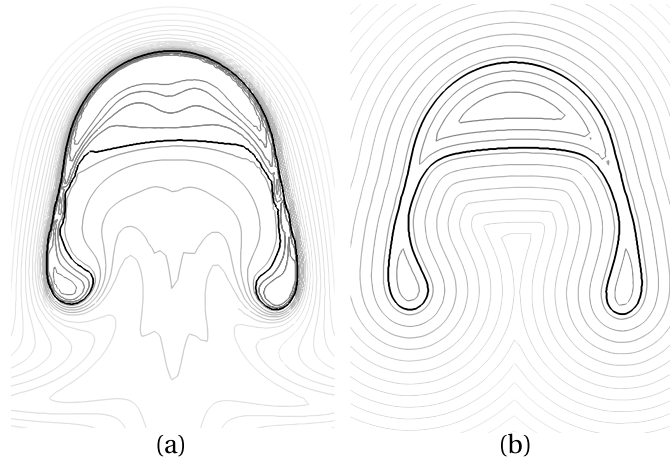
Fig. 1.5 – Schematic of the influence of level set regularisation on the distance function at the same time frame: a) without any regularisation step, the isovalue contours are distorted in the wake of the rising air bubble while being squeezed ahead of it, b) in contrast to regularising the distance function, where the contours maintain their spacing and geometric properties with respect to the tracked interface.

Classic Hamilton-Jacobi reinitialisation

In order to repair a distance function impaired by convective transport, Sussman et al. [1994] proposed solving a classic *Hamilton-Jacobi* equation, given in its most general form:

$$\frac{\partial \alpha}{\partial t} + \mathbb{H}(\alpha, x, t) = 0 \qquad x \in \Omega, t > 0 \tag{1.69}$$

where $\alpha(x, t = 0) = \alpha_0$ is the initial value of the distance function. The term $\mathbb{H}$ is known as the *Hamiltonian*. When the sign of the level set and its metric property ($\|\boldsymbol{\nabla}\alpha\| = 1$) are considered, eq. (1.69) reduces to:

$$\frac{\partial \alpha}{\partial t} + S(\alpha)\left(\|\boldsymbol{\nabla}\alpha\| - 1\right) = 0 \tag{1.70}$$

where $S(\alpha)$ is a step function giving the sign of the level set as follows:

$$S(\alpha) = \frac{\alpha}{|\alpha|} = \begin{cases} -1 & \text{if } \alpha < 0 \\ 0 & \text{if } \alpha = 0 \\ +1 & \text{if } \alpha > 0 \end{cases} \tag{1.71}$$

The sign function defined in eq. (1.71) is often smoothed to avoid numerical problems, as proposed for instance by Sussman et al. [1994]:

$$S(\alpha) = S_\varepsilon(\alpha) = \frac{\alpha}{\sqrt{\alpha^2 + \varepsilon^2}} \tag{1.72}$$

where ε is a smoothing parameter that depends on the mesh size around the interface. However, one should be aware that within the smoothing thickness, the regularised function may suffer from local oscillations because of the reciprocal reinitialisation taking place at each side of the level set. Peng et al. [1999] states that this problem is more likely to happen if the initial level set shows very weak or very steep gradients, and therefore is not regular enough. The authors eventually propose a new sign function which would reinitialise the distance function, as close as possible to the interface without modifying the latter, as follows:

$$S(\alpha) = S_\varepsilon(\alpha) = \frac{\alpha}{\sqrt{\alpha^2 + \|\boldsymbol{\nabla}\alpha\|^2 \varepsilon^2}} \tag{1.73}$$

Convective reinitialization

A recent work by Ville et al. [2011] introduced another concept for reinialisation called the *convective reinitialisation*. The idea lies in combining both level set advection and regularisation in a single equation, saving resolution time. The key components of their method starts by defining a pseudo time step, $\Delta\tau$, that is linked to the main time variable through a numerical parameter λ_τ, as follows:

$$\lambda_\tau = \frac{\partial \tau}{\partial t} \tag{1.74}$$

The order of magnitude of λ_τ, which can be seen as a relaxation parameter [see Vigneaux 2007, p. 89], is close to the ratio $h/\Delta t$. Then, the classic Hamilton-Jacobi eq. (1.69) is combined into the convection step by writing:

$$\frac{\partial \alpha}{\partial t} + (\boldsymbol{v} + \lambda_\tau \boldsymbol{U}) \cdot \boldsymbol{\nabla}\alpha = \lambda_\tau S(\alpha) \tag{1.75}$$

where $\boldsymbol{U}$ is a velocity vector in the normal direction to the interface, defined by $\boldsymbol{U} = S(\alpha)\boldsymbol{n}$. the normal vector $\boldsymbol{n}$ being previously defined in eq. (1.55). The obvious shortcoming of convective reinitialisation is that it depends on a numerical parameter λ_τ. Another limitation of the method is the use of a sinusoidal filter to modify the distance function by truncating its values beyond a thickness threshold, which is also another parameter to calibrate the resolution. The drawback of truncating the level set is the loss of information far from the interface and the inability to fully reconstruct the distance function. If we denote this threshold by E and the modified level set by $\widetilde{\alpha}$ inside the thickness, then eq. (1.75) is recast as:

$$\frac{\partial \alpha}{\partial t} + (\boldsymbol{v} + \lambda_\tau \boldsymbol{U}) \cdot \boldsymbol{\nabla}\alpha = \lambda_\tau S(\alpha)\sqrt{1 - \left(\frac{\pi}{2E}\widetilde{\alpha}\right)^2} \tag{1.76}$$

Equation (1.76) describes the transport and partial reconstruction of the distance function α, knowing its value $\widetilde{\alpha}$ inside the thickness E.

Geometric reinitialization

This category of methods go from the level set's basic geometric principle to construct a distance function, instead of solving a partial differential system of equations as in the classic Hamilton-Jacobi reinitialisation. A widely known instance of this category is the *fast marching method* developed by Sethian [1996] and influenced by the Dijkstra [1959]'s method to compute the shortest path in a network of nodes. The method aims to solve the eikonal equation in eq. (1.68) to propagate the distance function in a single direction by *upwinding*, i.e. going from low to high values of the distance function, while preserving a unitary distance gradient.

Direct reinitialisation is another interesting method in the geometric reinitialise category. However, it has not gained noticeable attention in the literature given the terrible cost in terms of computation time and efficiency if not optimised. The main idea is very simple: reconstruct the distance function over Ω ar a subset of Ω, by computing the minimum distance between each mesh node and the interface. It means that, for

any point $x \in \Omega$, the following constraint should be satisfied Osher and Fedkiw [2003]:

$$d_\Gamma(x) = \min\|x - x_\Gamma\| \qquad \forall x_\Gamma \in \partial\Omega = \Gamma, \qquad (1.77)$$

A efficient and optimised implementation of this method is done by Shakoor et al. [2015] making use of *k-d* trees to limit the search operations of elements and the subsequent distance evaluations in each of these elements. Moreover, the authors give a comparison of the previously stated methods on 2D and 3D cases, showing the great performance of direct reinitialisation when used with k-d trees algorithm, hence we use it in the present work.

1.6 Mesh adaptation

1.6.1 Metrics and anisotropy

The key to reduce spatial discretisation errors and obtain better results is a fine mesh. The optimal mesh resolution depends on the equations being discretised and solved on the FE grid, which consists of an array of structured triangles (fig. 1.6a), in the most basic situation. However, the potential of the Finite Element Method over other methods like the Finite Volume Method (FVM) is the use of unstructured grids. The easiest meshing solution one can choose is to create unstructured homogeneous and isotropic grid (fig. 1.6b), while respecting some constraints regarding the time step (temporal discretisation) stemming from physical or numerical conditions, e.g. diffusion shock constraint in diffusional transient equations or Courant–Friedrichs–Lewy (CFL) condition in transient advective equations. In such a case, errors due to interpolation are minimised, which guaranties good results but with expensive time cost. Heterogeneous meshes (fig. 1.6c) that consist of fine isotropic elements in areas of interest along with coarser isotropic elements in other areas, may reduce the needed time to solver each conservation equation. Although this is an interesting alternative, it is less powerful than anisotropic meshing. In the latter (fig. 1.6d), elements adapt to a physical quantity, such as enthalpy or velocity, reducing the elemental length in the direction where the gradient is higher, while stretching the element in the orthogonal direction. This allows more accurate resolution with less elements than needed by isotropic meshing. Moreover, this type of meshing is well adapted to the context of this thesis as it allows getting a fine mesh in the normal direction to the interface, that is in its transport direction, while reducing the number of elements in other directions. Regions undergoing solidification are also important to remesh since microsegregation starts in the mushy zone, i.e. between the liquidus and solidus temperatures

given by a local average composition, where fluid flow may transport species, leading eventually to macrosegregation.
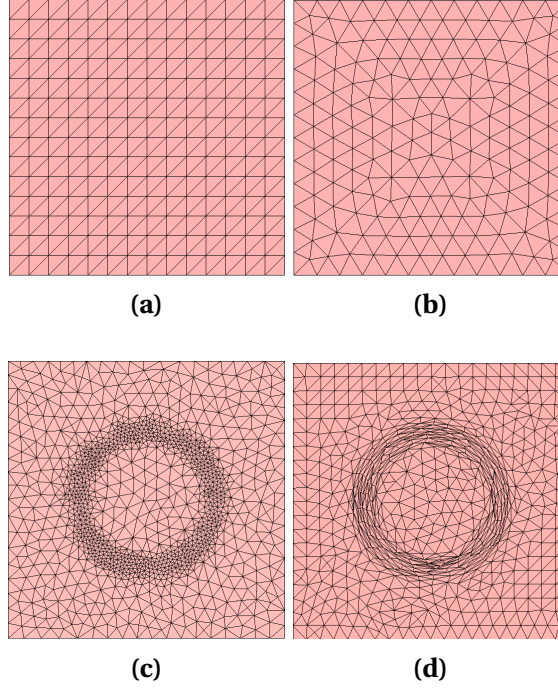

Fig. 1.6 – Alternatives for initial finite element grid generation: (a) structured homogeneous, (b) unstructured homogeneous isotropic, (c) unstructured heterogeneous isotropic and (d) unstructured heterogeneous anisotropic meshes.

Since mesh adaptation involves advanced mathematical notions, readers interested in the basics are referred to the following references: [Coupez 1991; Coupez 2000; Gruau and Coupez 2005; Jannoun 2014]. In this study, we show and compare different remeshing methods relevant to macrosegregation prediction, and based on previous work done at CEMEF. These techniques rely on metric tensors, and some of them belong to *a posteriori* error estimators category. A metric or a metric tensor $\mathcal{M}$, also known as *Riemannian* metric, is a positive symmetric definite matrix that relates to an element's size in $\mathbb{R}^3$ via:

$$\mathcal{M} = \begin{pmatrix} M_{11} & M_{12} & M_{13} \\ M_{12} & M_{22} & M_{23} \\ M_{13} & M_{23} & M_{33} \end{pmatrix} = \mathcal{R} \begin{pmatrix} 1/h_x^2 & 0 & 0 \\ 0 & 1/h_y^2 & 0 \\ 0 & 0 & 1/h_z^2 \end{pmatrix} \mathcal{R}^T \qquad (1.78)$$

where $\mathcal{R}$ is a rotation matrix and h_x, h_y and h_z are the respective dilatation scalars defined by the metric in the (x, y, z) space, describing a three-dimensional anisotropy. The metric information is then passed to a mesh generation tool, called *MTC*, which is based on an iterative procedure of local topology optimisations. We focus hereafter

on two adaptive remeshing techniques, then discuss the functional details and show some examples.

1.6.2 *Remesh2*: Interface remeshing

Remesh2 is an explicit method to compute an anisotropic metric around the zero surface of a distance function. The idea is, as mentioned previously, to reduce the elements cost in the tangential directions to level set by stretching the elements, leaving small element lengths in the normal direction, where the level set gradient is the greatest. This method is not based on error estimators, but rather on explicit input from the user who chooses the mesh size in normal and tangential directions to the interface, as well as in the positive and negative regions delimited by the level set. The following parameters are used as input data to determine the final node-wise metric:

$h_{\boldsymbol{n}}$ mesh size in the normal direction of the level set

$h_{\boldsymbol{\tau}}$ mesh size in the tangential directions of the level set

h_M mesh size in the metal

h_A mesh size in the air

α distance function (level set)

ε level set mixing thickness

$\boldsymbol{V}$ arbitrary vector

Algorithm 1: *Remesh2* metric construction

Data: $\boldsymbol{n}$ h_M h_A $h_{\boldsymbol{n}}$ $h_{\boldsymbol{\tau}}$ α

Result: $\mathcal{M}_2$

Initialise node index: $j = 0$;

while $j \leq j_{end}$ **do**

  if $\alpha_j < \varepsilon$ **then**

    Compute normal direction to level set: $\boldsymbol{n} = \boldsymbol{\nabla}\alpha / \|\boldsymbol{\nabla}\alpha\|$;

    Compute the first tangential direction: $\boldsymbol{\tau_1} = \boldsymbol{V} - (\boldsymbol{V} \cdot \boldsymbol{n}) \cdot \boldsymbol{n}$;

    Deduce the second tangential direction: $\boldsymbol{\tau_2} = \boldsymbol{n} \wedge \boldsymbol{\tau_1}$;

    Compute rotation matrix and its transpose: $\mathcal{R}_j$ and $\mathcal{R}_j^{-1}$;

    Deduce P1 metric at node j: $(\mathcal{M}_2)_j = \mathcal{R}_j \Lambda \mathcal{R}_j^{-1}$

  else

    go back to the beginning of current section;

  Increment j ;

1.6.3 *Remesh4*: **Multi-criteria remeshing**

It is a metric construction method based on edge-based error distribution

What i concluded from Z-FAST-SMACS cases A and B, where remesh4 was used in two different ways (LS and velocity/100 , LS and ConcentrationPosNeg) is that for diffuse interface thickness less than 2e-4 m, mass conservation gets all sorts of problems, because of low element resolution around interface while higher resolution at the tips of the transition region

To do ?

Interface Remeshing: Importance when using a static level set and more importantly when LS is transported, influence of mixing area *thickness* and *resolution* (i.e. nb of nodes with the area), Isotropic or anisotropic ? the first is more important to composition calculation while the second is more relevant if we mean do thermohydraulics without macrosegregation

Résumé chapitre 2

Le second chapitre de ce manuscrit présente une revue de la littérature, concernant les aspects de modélisation utilisés dans ce travail. Au début, on présente quelques approches connues pour modéliser l'effet de la microségrégation sur la variation des fractions de phases ainsi que leurs compositions. On s'intéresse après à l'approche de prise de moyenne volumique. Celle-ci nous permet de faire des hypothèses sur des petits volumes, qualifiés de *volumes élémentaires représentatifs*, permettant d'établir des relations pour l'ensemble des propriétés des phases. En utilisant ces relations, on présente la première brique numérique de ce travail : les équations de conservation de masse, énergie, solutés et quantité de mouvement dans un contexte de solidification à volume constant, donc sans retrait. Le modèle est complété par une hypothèse de solide fixe et rigide qui permet de négliger tout movement des phases solides, et donc la thermomécanique de ces phases n'est pas traitée. Dans la suite du chapitre, on présente les descriptions eulérienne et lagrangienne caractérisant l'écoulement de la phase liquide. Cela s'avère nécessaire dans un contexte de solidification avec changement de volume, où l'interface entre le métal et le milieu ambiant change au cours de la transformation. Par conséquent, le choix de la méthode level set pour le suivi de cette interface est expliqué. On présente aussi des méthodes numériques pour prendre en compte le mouvement de l'interface suivie par la méthode level set, dans le contexte eulérien. Finalement, deux méthodes de remaillage adaptatif, utilisé pour l'ensemble des calculs faits pendant la thèse, sont présentés et expliqués, tout en montrant leurs avantages et leurs inconvénients.

Bibliography

[Basset 2006]

Basset, O. (2006). "Simulation numérique d'écoulements multi-fluides sur grille de calcul". PhD Thesis. École Nationale Supérieure des Mines de Paris. URL: `https://tel.archives-ouvertes.fr/tel-00376484` (cited on page 20).

[Beckermann et al. 1999]

Beckermann, C, Diepers, H. J, Steinbach, I, Karma, A, and Tong, X (1999). "Modeling Melt Convection in Phase-Field Simulations of Solidification". *Journal of Computational Physics,* 154 (2), pp. 468–496. URL: `http://www.sciencedirect.com/science/article/pii/S0021999199963234` (cited on pages 12, 15).

[Boettinger et al. 2002]

Boettinger, W. J., Warren, J. A., Beckermann, C., and Karma, A. (2002). "Phase-Field Simulation of Solidification1". *Annual Review of Materials Research,* 32 (1), pp. 163–194. URL: `http://dx.doi.org/10.1146/annurev.matsci.32.101901.155803` (cited on page 13).

[Brackbill et al. 1992]

Brackbill, J. U, Kothe, D. B, and Zemach, C (1992). "A continuum method for modeling surface tension". *Journal of Computational Physics,* 100 (2), pp. 335–354. URL: `http://www.sciencedirect.com/science/article/pii/002199919290240Y` (cited on page 15).

[Brody and Flemings 1966]

Brody, H. D. and Flemings, M. C. (1966). "Solute redistribution in denritic solidification". *AIME Met. Soc. Trans.,* 236, p. 615 (cited on page 3).

[Brooks and Hughes 1982]

Brooks, A. N. and Hughes, T. J. R. (1982). "Streamline upwind/Petrov-Galerkin formulations for convection dominated flows with particular emphasis on the incompressible Navier-Stokes equations". *Computer Methods in Applied Mechanics and Engineering,* 32 (1–3), pp. 199–259. URL: `http://www.sciencedirect.com/science/article/pii/0045782582900718` (cited on page 19).

[Chen et al. 1997]

Chen, S., Merriman, B., Osher, S., and Smereka, P. (1997). "A Simple Level Set Method for Solving Stefan Problems". *Journal of Computational Physics,* 135 (1), pp. 8–29. URL: `http://www.sciencedirect.com/science/article/pii/S0021999197957211` (cited on page 13).

[Chen 2014]

Chen, S. (2014). "Three dimensional Cellular Automaton - Finite Element (CAFE) modeling for the grain structures development in Gas Tungsten / Metal Arc Welding processes". PhD thesis. Ecole

Bibliography

Nationale Supérieure des Mines de Paris. URL: https://pastel.archives-ouvertes.fr/pastel-01038028/document (cited on page 13).

[Clyne and Kurz 1981]
Clyne, T. W. and Kurz, W. (1981). "Solute redistribution during solidification with rapid solid state diffusion". *Metallurgical Transactions A,* 12 (6), pp. 965–971. URL: http://link.springer.com/article/10.1007/BF02643477 (cited on page 3).

[Combeau et al. 1996]
Combeau, H., Drezet, J.-M., Mo, A., and Rappaz, M. (1996). "Modeling of microsegregation in macrosegregation computations". *Metallurgical and Materials Transactions A,* 27 (8), pp. 2314–2327. URL: http://link.springer.com/article/10.1007/BF02651886 (cited on page 3).

[Coupez 1991]
Coupez, T. (1991). *Grandes transformations et remaillage automatique.* EMP. URL: http://www.theses.fr/1991ENMP0615 (cited on page 25).

[Coupez 2000]
Coupez, T. (2000). "Génération de maillage et adaptation de maillage par optimisation locale". *Revue Européenne des Éléments,* 9 (4), pp. 403–423. URL: http://www.tandfonline.com/doi/abs/10.1080/12506559.2000.10511454 (cited on page 25).

[Courtois et al. 2014]
Courtois, M., Carin, M., Masson, P. L., Gaied, S., and Balabane, M. (2014). "A complete model of keyhole and melt pool dynamics to analyze instabilities and collapse during laser welding". *Journal of Laser Applications,* 26 (4), p. 042001. URL: http://scitation.aip.org/content/lia/journal/jla/26/4/10.2351/1.4886835 (cited on page 13).

[Dantzig and Rappaz 2009]
Dantzig, J. A. and Rappaz, M. (2009). *Solidification.* EPFL Press (cited on pages 3, 4, 8).

[Desmaison et al. 2014]
Desmaison, O., Bellet, M., and Guillemot, G. (2014). "A level set approach for the simulation of the multipass hybrid laser/GMA welding process". *Computational Materials Science,* 91, pp. 240–250. URL: http://www.sciencedirect.com/science/article/pii/S092702561400278X (cited on page 13).

[Dijkstra 1959]
Dijkstra, E. W. (1959). "A note on two problems in connexion with graphs". *Numerische Mathematik,* 1 (1), pp. 269–271. URL: http://link.springer.com/article/10.1007/BF01386390 (cited on page 23).

[Du et al. 2001]
Du, Q., Li, D., Li, Y., Li, R., and Zhang, P. (2001). "Simulating a double casting technique using level set method". *Computational Materials Science,* 22 (3–4), pp. 200–212. URL: http://www.sciencedirect.com/science/article/pii/S0927025601001902 (cited on page 13).

[Ettrich et al. 2014]
Ettrich, J., Choudhury, A., Tschukin, O., Schoof, E., August, A., and Nestler, B. (2014). "Modelling of transient heat conduction with diffuse interface methods". *Modelling and Simulation in Materials*

Science and Engineering, 22 (8), p. 085006. URL: http://iopscience.iop.org/0965-0393/22/8/085006 (cited on page 17).

[Gada and Sharma 2009]

Gada, V. H. and Sharma, A. (2009). "On Derivation and Physical Interpretation of Level Set Method–Based Equations for Two-Phase Flow Simulations". *Numerical Heat Transfer, Part B: Fundamentals,* 56 (4), pp. 307–322. URL: http://dx.doi.org/10.1080/10407790903388258 (cited on page 15).

[Gibou et al. 2003]

Gibou, F., Fedkiw, R., Caflisch, R., and Osher, S. (2003). "A Level Set Approach for the Numerical Simulation of Dendritic Growth". *Journal of Scientific Computing,* 19 (1-3), pp. 183–199. URL: http://link.springer.com/article/10.1023/A%3A1025399807998 (cited on page 13).

[Gruau and Coupez 2005]

Gruau, C. and Coupez, T. (2005). "3D tetrahedral, unstructured and anisotropic mesh generation with adaptation to natural and multidomain metric". *Computer Methods in Applied Mechanics and Engineering,* Unstructured Mesh Generation 194 (48–49), pp. 4951–4976. URL: http://www.sciencedirect.com/science/article/pii/S0045782505000745 (cited on page 25).

[Harlow and Welch 1965]

Harlow, F. H. and Welch, J. E. (1965). "Numerical Calculation of Time-Dependent Viscous Incompressible Flow of Fluid with Free Surface". *Physics of Fluids (1958-1988),* 8 (12), pp. 2182–2189. URL: http://scitation.aip.org/content/aip/journal/pof1/8/12/10.1063/1.1761178 (cited on page 12).

[Hirt 1971]

Hirt, C. W. (1971). "An arbitrary Lagrangian-Eulerian computing technique". *Proceedings of the Second International Conference on Numerical Methods in Fluid Dynamics.* Ed. by M. Holt. Lecture Notes in Physics 8. Springer Berlin Heidelberg, pp. 350–355. URL: http://link.springer.com/chapter/10.1007/3-540-05407-3_50 (cited on page 12).

[Hirt and Nichols 1981]

Hirt, C. W and Nichols, B. D (1981). "Volume of fluid (VOF) method for the dynamics of free boundaries". *Journal of Computational Physics,* 39 (1), pp. 201–225. URL: http://www.sciencedirect.com/science/article/pii/0021999181901455 (cited on page 12).

[Hysing et al. 2009]

Hysing, S., Turek, S., Kuzmin, D., Parolini, N., Burman, E., Ganesan, S., and Tobiska, L. (2009). "Quantitative benchmark computations of two-dimensional bubble dynamics". *International Journal for Numerical Methods in Fluids,* 60 (11), pp. 1259–1288. URL: http://onlinelibrary.wiley.com/doi/10.1002/fld.1934/abstract (cited on page 20).

[Jannoun 2014]

Jannoun, G. E. (2014). "Space-Time accurate anisotropic adaptation and stabilized finite element methods for the resolution of unsteady CFD problems". PhD thesis. Ecole Nationale Supérieure des Mines de Paris. URL: https://pastel.archives-ouvertes.fr/tel-01146245/document (cited on page 25).

[Karma and Rappel 1996]

Karma, A. and Rappel, W.-J. (1996). "Phase-field method for computationally efficient modeling

Bibliography

of solidification with arbitrary interface kinetics". *Physical Review E,* 53 (4), R3017–R3020. URL: http://link.aps.org/doi/10.1103/PhysRevE.53.R3017 (cited on pages 12, 13).

[Kobayashi 1988]
Kobayashi, S. (1988). "Solute redistribution during solidification with diffusion in solid phase: A theoretical analysis". *Journal of Crystal Growth,* 88 (1), pp. 87–96. URL: http://www.sciencedirect.com/science/article/pii/S0022024898900100 (cited on page 3).

[Maitre 2006]
Maitre, E. (2006). "Review of numerical methods for free interfaces". Les Houches, France. URL: http://goo.gl/Re6f3a (cited on page 12).

[Martorano et al. 2003]
Martorano, M. A., Beckermann, C., and Gandin, C.-A. (2003). "A solutal interaction mechanism for the columnar-to-equiaxed transition in alloy solidification". *Metallurgical and Materials Transactions A,* 34 (8), pp. 1657–1674. URL: http://link.springer.com/article/10.1007/s11661-003-0311-x (cited on page 3).

[Ni and Beckermann 1991]
Ni, J. and Beckermann, C. (1991). "A volume-averaged two-phase model for transport phenomena during solidification". *Metallurgical Transactions B,* 22 (3), pp. 349–361. URL: http://link.springer.com/article/10.1007/BF02651234 (cited on pages 3, 4, 6).

[Osher and Fedkiw 2003]
Osher, S. and Fedkiw, R. (2003). "Signed Distance Functions". *Level Set Methods and Dynamic Implicit Surfaces.* Applied Mathematical Sciences 153. Springer New York, pp. 17–22. URL: http://link.springer.com/chapter/10.1007/0-387-22746-6_2 (cited on page 24).

[Osher and Sethian 1988]
Osher, S. and Sethian, J. A. (1988). "Fronts propagating with curvature-dependent speed: Algorithms based on Hamilton-Jacobi formulations". *Journal of Computational Physics,* 79 (1), pp. 12–49. URL: http://www.sciencedirect.com/science/article/pii/0021999188900022 (cited on pages 12, 13).

[Peng et al. 1999]
Peng, D., Merriman, B., Osher, S., Zhao, H., and Kang, M. (1999). "A PDE-Based Fast Local Level Set Method". *Journal of Computational Physics,* 155 (2), pp. 410–438. URL: http://www.sciencedirect.com/science/article/pii/S0021999199963453 (cited on pages 16, 22).

[Prosperetti 2002]
Prosperetti, A. (2002). "Navier-Stokes Numerical Algorithms for Free-Surface Flow Computations: An Overview". *Drop-Surface Interactions.* Ed. by M. Rein. CISM International Centre for Mechanical Sciences 456. Springer Vienna, pp. 237–257. URL: http://link.springer.com/chapter/10.1007/978-3-7091-2594-6_8 (cited on page 12).

[Sethian 1996]
Sethian, J. A. (1996). "A fast marching level set method for monotonically advancing fronts". *Proceedings of the National Academy of Sciences,* 93 (4), pp. 1591–1595. URL: http://www.pnas.org/content/93/4/1591 (cited on page 23).

[Shakoor et al. 2015]

Shakoor, M., Scholtes, B., Bouchard, P.-O., and Bernacki, M. (2015). "An efficient and parallel level set reinitialization method - Application to micromechanics and microstructural evolutions". *Applied Mathematical Modelling (submitted),* (cited on page 24).

[Strotos et al. 2008]

Strotos, G., Gavaises, M., Theodorakakos, A., and Bergeles, G. (2008). "Numerical investigation of the cooling effectiveness of a droplet impinging on a heated surface". *International Journal of Heat and Mass Transfer,* 51 (19–20), pp. 4728–4742. URL: http://www.sciencedirect.com/science/article/pii/S001793100800149X (cited on page 17).

[Sun and Beckermann 2004]

Sun, Y. and Beckermann, C. (2004). "Diffuse interface modeling of two-phase flows based on averaging: mass and momentum equations". *Physica D: Nonlinear Phenomena,* 198 (3–4), pp. 281–308. URL: http://www.sciencedirect.com/science/article/pii/S0167278904003689 (cited on page 15).

[Sussman et al. 1994]

Sussman, M., Smereka, P., and Osher, S. (1994). "A Level Set Approach for Computing Solutions to Incompressible Two-Phase Flow". *Journal of Computational Physics,* 114 (1), pp. 146–159. URL: http://www.sciencedirect.com/science/article/pii/S0021999184711557 (cited on pages 20–22).

[Tan and Zabaras 2007]

Tan, L. and Zabaras, N. (2007). "A level set simulation of dendritic solidification of multi-component alloys". *Journal of Computational Physics,* 221 (1), pp. 9–40. URL: http://www.sciencedirect.com/science/article/pii/S0021999106002737 (cited on page 13).

[Tourret and Gandin 2009]

Tourret, D. and Gandin, C. A. (2009). "A generalized segregation model for concurrent dendritic, peritectic and eutectic solidification". *Acta Materialia,* 57 (7), pp. 2066–2079. URL: http://www.sciencedirect.com/science/article/pii/S1359645409000184 (cited on page 3).

[Vigneaux 2007]

Vigneaux, P. (2007). "Méthodes Level Set pour des problèmes d'interface en microfluidique". PhD thesis. Université Sciences et Technologies - Bordeaux I. URL: https://tel.archives-ouvertes.fr/tel-00189409/document (cited on page 23).

[Ville et al. 2011]

Ville, L., Silva, L., and Coupez, T. (2011). "Convected level set method for the numerical simulation of fluid buckling". *International Journal for Numerical Methods in Fluids,* 66 (3), pp. 324–344. URL: http://onlinelibrary.wiley.com/doi/10.1002/fld.2259/abstract (cited on page 22).

[Wang and Beckermann 1993]

Wang, C. Y. and Beckermann, C. (1993). "A multiphase solute diffusion model for dendritic alloy solidification". *Metallurgical Transactions A,* 24 (12), pp. 2787–2802. URL: http://link.springer.com/article/10.1007/BF02659502 (cited on page 3).

Modélisation par Level Set des macroségrégations induites par le retrait à la solidification

RESUME : La macroségrégation est un défaut connu dans les procédés de coulées industrielles. La genèse de ce défaut est la conséquence de l'interaction complexe entre la microségrégation ou la distribution des espèces chimiques à l'échelle de la microstructure et les mouvements des phases liquide et solides. Les hétérogéneités de concentration en solutés à l'échelle de la pièce peuvent être rédhibitoires vis-à-vis de la qualité du produit. Dans ce travail, on propose un modèle numérique pour simuler et prédire la formation des macroségrégations en coeur des pièces d'alliages multi-constitués, induites par des variations thermiques et solutales dans la phase liquide. Dans un premier temps, on considère que le métal solidifie à volume constant. Dans ce contexte, la convection thermosolutale est étudiée ainsi que son influence sur la formation des canaux ségrégés à différentes échelles de modélisation. Dans un deuxième temps, le modèle vise à prédire les macroségrégations en présence de changement de volume du métal, dont la cause principale est le retrait à la solidification, pouvant être à l'origine du phénomène de ségrégation inverse. La surface entre le métal et le gaz environnant au cours du retrait évolue pendant le retrait en fonction du chemin de solidification qui varie avec la macroségrégation. Cette évolution d'interface est suivie par la méthode Level set. Des prédictions de concentration moyenne, couplées aux bases de données thermodynamiques pour mieux prédire les chemins de solidification des alliages multi-constitués, sont analysées et comparées avec des résultats expérimentaux. Finalement, des calculs de solidification en microgravité sont présentées, simulant un essai expérimental dans le contexte du projet CCEMLCC lancé par l'Agence Spatiale Européenne. Les résultats en fin de solidification montrent un accord acceptable quant à la forme et l'élongation des échantillons solidifiées. Ces calculs sont faits avec des approximations binaire, ternaire et quaternaire d'une même nuance d'acier utilisée dans les essais en microgravité.

Mots clés : modélisation,solidification,ségrégation,Level Set,éléments finis,métallurgie

Numerical modeling of macrosegregation formed during solidification with shrinkage using a Level Set Approach

ABSTRACT : Macrosegregation is key defect in industrial casting processes. During solidification, solute redistribution at the scale of microstructure, also known as microsegregation, take place with complex interactions, in order to form one or more solid phases. These interactions between microsegregation and movements of liquid and solid phases may lead to macrosegregations. These solute heterogeneities spanning on a larger scale, may result in a bad casting quality. In this thesis, we propose a numerical model to simulate and predict macrosegregations occurring in the centre of multicomponent alloys, caused by thermal and solutal variations in the liquid phase. First, we assume that the metallic alloy solidifies with a constant volume. In this context, we study the influence of thermosolutal convection on the formation of channel segregations, at different modelling scales. The second part of this modelling work consider solidification while the metallic alloy's volume is decreasing, mainly due to overall density variation, also known as solidification shrinkage, possibly leading to the so-called inverse segregation phenomenon, appearing on the alloy's skin. In the context of solidification shrinkage, the shape of the metal's boundary with surrounding gases varies according to a constantly changing solidification path due to macrosegregation. The Level Set method is therefore used to track its evolution with time. Composition predictions, coupled with thermodynamic database mappings for more accurate multicomponent solidification paths, are analysed and compared to existing experimental setups. Finally, simulations of a reduced-gravity solidification cases are performed, mocking an experimental benchmark from the CCEMLCC project launched by the European Space Agency. The results show acceptable agreement for the final shape, compared to experimental results. These computations were performed with binary, ternary and quaternary approximations of the same steel grade which was used in reduced-gravity experiments.

Keywords : modelling, solidification, segregation, Level Set, finite elements, metallurgy

MINES ParisTech

ParisTech
INSTITUT DES SCIENCES ET TECHNOLOGIES
PARIS INSTITUTE OF TECHNOLOGY